The Role of Water in Gas Hydrate Dissociation

Susan Circone,* Laura A. Stern, and Stephen H. Kirby

U.S. Geological Survey, 345 Middlefield Road MS 977, Menlo Park, California 94025

Received: August 1, 2003; In Final Form: February 27, 2004

When raised to temperatures above the ice melting point, gas hydrates release their gas in well-defined, reproducible events that occur within self-maintained temperature ranges slightly below the ice point. This behavior is observed for structure I (carbon dioxide, methane) and structure II gas hydrates (methane−ethane, and propane), including those formed with either H_2O- or D_2O-host frameworks, and dissociated at either ambient or elevated pressure conditions. We hypothesize that at temperatures above the H_2O (or D_2O) melting point: (1) hydrate dissociation produces water + gas instead of ice + gas, (2) the endothermic dissociation reaction lowers the temperature of the sample, causing the water product to freeze, (3) this phase transition buffers the sample temperatures within a narrow temperature range just below the ice point until dissociation goes to completion, and (4) the temperature depression below the pure ice melting point correlates with the average rate of dissociation and arises from solution of the hydrate-forming gas, released by dissociation, in the water phase at elevated concentrations. In addition, for hydrate that is partially dissociated to ice + gas at lower temperatures and then heated to temperatures above the ice point, all remaining hydrate dissociates to gas + liquid water as existing barriers to dissociation disappear. The enhanced dissociation rates at warmer temperatures are probably associated with faster gas transport pathways arising from the formation of water product.

Introduction

When gas hydrate is in surroundings maintained at temperatures above the ice melting point and pressure is then reduced to 0.1 MPa, rapid dissociation occurs and sample temperatures decrease. This phenomenon has been observed in both natural and experimental systems. Marine drill core material containing gas hydrate is often recovered at temperatures several degrees below the measured temperature at the core site.[1−3] Temperatures can be depressed as much as 2 degrees below the ice point and are significantly lower than any encountered during core retrieval. Such thermal anomalies arise from the endothermic enthalpy of hydrate dissociation and are used routinely as indicators of the possible presence of hydrate in recovered cores.

We previously reported that under certain conditions at 0.1 MPa, structure I (sI) methane hydrate dissociates in a self-maintained, fixed temperature range within −1.5 K of the pure H_2O melting point (273.15 K) until the reaction goes to completion.[4,5] Specifically, this was observed when samples of methane (C1) hydrate were rapidly depressurized to 0.1 MPa while maintained in an external fluid bath held at a fixed temperature at or above 273 K.[4] This thermal buffering behavior was found to be independent of the external bath temperature, which ranged between 273 and 289 K. Similar behavior was observed when partially dissociated C1 hydrate samples were heated from low temperature through T_m at 0.1 MPa,[5] where T_m is defined as the melting point of the ice that comprises the hydrate framework (H_2O or D_2O). In these experiments, this thermal buffering behavior and the release of all remaining gas were observed regardless of sample history, the prior rate of dissociation, or the extent of partial dissociation.

We have now observed similar thermal buffering behavior during dissociation of sI carbon dioxide (CO_2) hydrate,[6] as well as structure II (sII) methane−ethane hydrate (C1C2) and sII propane (C3) hydrate at 0.1 MPa. In CO_2 hydrate dissociation experiments, the measured temperature depression below T_m was even greater, while C1C2 and C3 hydrate dissociation tests yielded results consistent with those described above for C1. Recent investigation of C1 hydrate dissociation at elevated pressures of 1 and 2 MPa also yielded results fully consistent with the earlier 0.1 MPa tests. Here we summarize the relationship between hydrate dissociation and buffering temperature for these various hydrates near T_m (the melting point of H_2O, or D_2O when noted) and provide a probable explanation for the observed behavior based on these observations.

Experimental Method

Pure, porous hydrate samples were synthesized using the method of Stern et al.[5,7] Pressurized hydrate-forming gas (or liquid) is introduced into a sample chamber containing granular ice (H_2O or D_2O, 180−250 μm grain size) packed to a nominal porosity of 40 to 55%. Hydrate formation is promoted by ramping temperature from 250 K to well above T_m, but still within the hydrate stability field. Samples are then maintained for several hours at the peak high-pressure, high-temperature conditions and/or cycled through T_m until the remaining seed ice has been converted to hydrate. Complete conversion of ice to hydrate is confirmed by the absence of abrupt pressure and temperature increases associated with water freezing when the samples are cooled through T_m after synthesis. Details of sample synthesis, experimental setup, and hydrate compositions have been reported previously for methane,[7,8] 0.8 methane−0.2 ethane,[9,10] propane,[11] and carbon dioxide[6] hydrates made by this general method. Hydrate samples were typically grown from

* Corresponding author. Tel: 650/329-5674. Fax: 650/329-5163. E-mail: scircone@usgs.gov.

10.1021/jp0362584 CCC: $27.50
Published on Web 04/14/2004

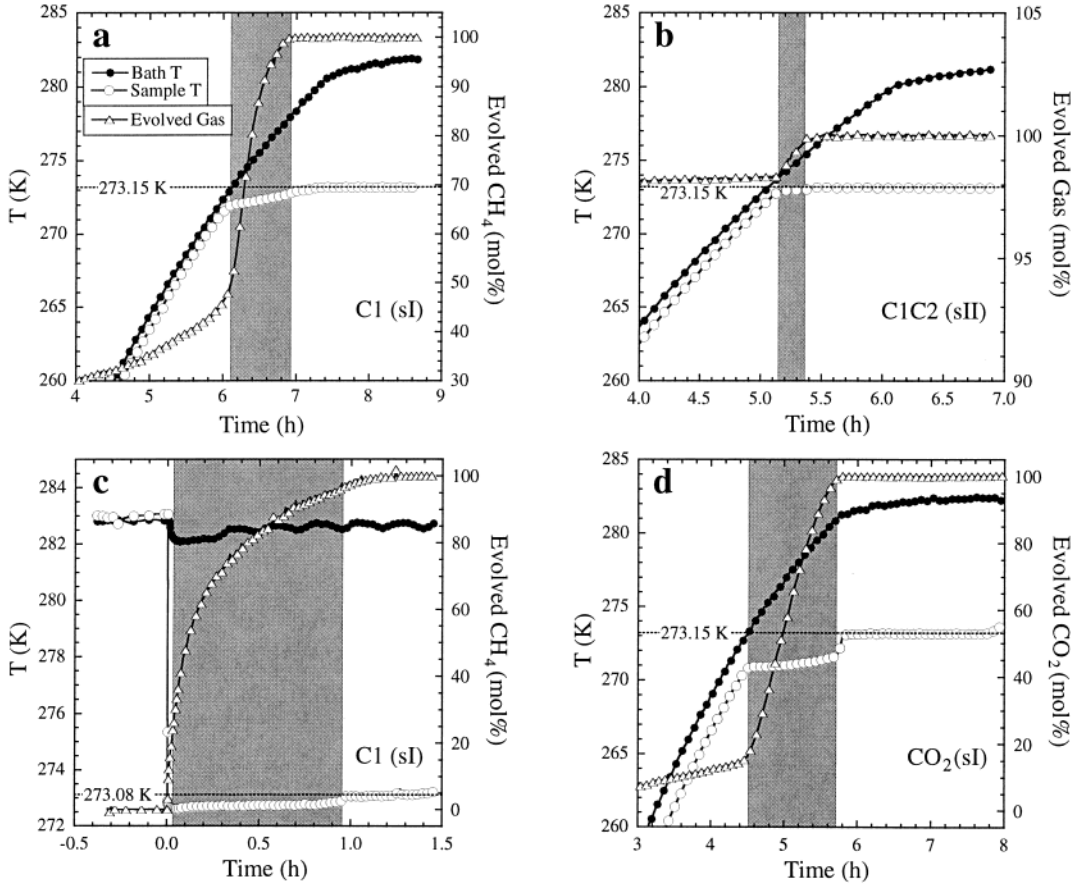

Figure 1. Evolution of gas from hydrate samples as a function of time and temperature, while warming the samples through T_m (panels a, b, d) or holding them at a fixed external temperature above T_m (panel c). Bath and sample middle temperatures (solid and open circles, respectively) and the amount of gas released from the hydrate sample (open triangles) are shown (every fifth data point plotted). Shaded regions indicate where the buffering *T* range has been defined. The horizontal dotted line indicates T_m for H_2O (experiment in panel c performed at 1.0 MPa). Note that during heating, the sample temperature lags the external bath temperature due to delayed heat transfer through the vessel walls and sample. Panel a shows the final temperature-scanning portion of a C1 hydrate dissociation experiment following a rapid depressurization to 0.1 MPa and isothermal hold at 245 K. Note that more than half of the hydrate gas content was released in the buffering temperature range. Panel b shows the final temperature-scanning portion of a C1C2 hydrate dissociation experiment following warming from 195 K at 0.1 MPa. The results are representative of all temperature-scanning experiments on C1, C1C2, and C3 gas hydrates in which only a few percent of the gas remains as T_m is approached. Panel c shows a fixed-temperature experiment on C1 hydrate following rapid depressurization to 1.0 MPa and isothermal hold at 283 K. Most of the hydrate sample dissociated in the buffering temperature range. The results are representative of fixed-temperature experiments above T_m on C1 hydrate at 0.1 MPa and elevated pressures. Panel d shows the final temperature-scanning portion of a CO_2 hydrate dissociation experiment following warming from 210 K at 0.1 MPa. The buffering temperature range shown is representative of all temperature-scanning and rapid depressurization (below and above T_m) experiments on CO_2 hydrate, in which the offset from T_m is greater than in panels a, b, or c.

26 g of H_2O seed ice in approximately 2.54 cm × 11 cm long cylinders. They contained 30 to 48% intergranular porosity depending on initial ice porosity. In addition, hydrate samples were made from D_2O ice, sample size was varied (initial mass of H_2O seed ice ranged from 16 to 30 g), and 100 μm quartz sand was mixed homogeneously or layered with C1 hydrate. One sample was a 3.18 cm-diameter cylinder made with 55 g of H_2O seed ice.

In this report we focus on the dissociation behavior of gas hydrate near T_m. Dissociation was monitored under two types of conditions: (1) during warming through T_m (temperature scanning), and (2) at fixed bath temperatures above T_m. In temperature-scanning experiments, the hydrate sample is actively warmed from a given starting temperature through T_m while a constant gas pressure is maintained. Heat to the sample is provided by an external fluid bath in which the sample chamber is immersed, and bath heating rates average 13 K/h.[4,6,7] A final bath temperature of 283 K was reached routinely, as all remaining gas has been released from the hydrate sample by this temperature. Temperature-scanning experiments include those that start in the hydrate equilibrium field at 0.1 MPa (referred to as temperature-ramping in refs 5,6,12) as well as others that initially start inside the hydrate equilibrium field at elevated pressure and some externally fixed temperature (T_{ext}) below T_m. These latter samples follow a pathway of rapid depressurization (~15 s to 0.1, 1 or 2 MPa) followed by an isothermal hold that ranges from <30 min to several weeks, during which time they undergo partial dissociation. Samples are then warmed through T_m and dissociate to completion. In fixed-temperature experiments, samples are equilibrated at elevated pressure and at a T_{ext} above T_m, then rapidly depressurized and held isothermally until the hydrate sample dissociates completely.

Sample dissociation rates were determined using our custom-built flow meter,[8] in which released gas is collected at 0.1 MPa. The gas flow rate is determined by monitoring the change in weight of an inverted, H_2O-filled, close-ended cylinder as released gas displaces the H_2O. The flow rate measurement capability ranges from 3000 to less than 0.1 cm^3/min. For dissociation experiments performed at elevated pressures, a

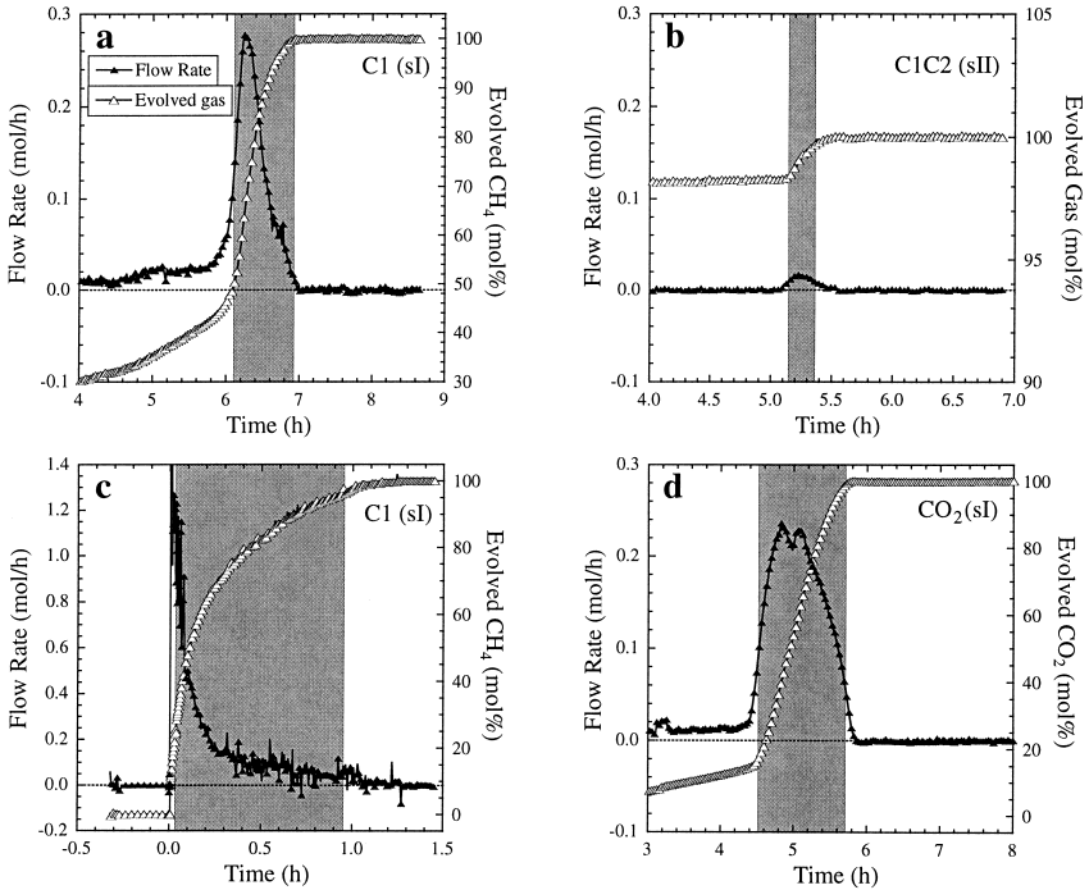

Figure 2. Experiments shown in Figure 1 plotted as the amount and rate of gas evolution over time, while warming the hydrate samples through T_m (panels a, b, d), or holding them at a fixed external temperature above T_m (panel c). The flow rate and evolved gas (solid and open triangles, respectively; every second data point plotted), the zero flow rate horizon (horizontal dotted line), and the buffering temperature range (shaded area, see Figure 1) are shown. Data were collected every 60 s except for that in panel c, where data were collected every 20 s. The flow rate was calculated at each data point from the change in amount of released gas (using a running average of nine points to reduce noise) over time. In temperature-scanning experiments (panels a, b, d), the initial and final buffering temperatures coincide with the breaks in the slopes of the gas evolution curves, while the flow rate changes are spread over a wider temperature range due to the data averaging. A temporal offset of up to 20 min between the onset of buffering and the peak in flow rate can occur.

back-pressure regulator (Tescom Model ER 3000), situated between the sample and the flow meter, maintains the pressure in the sample vessel to within ±0.03 MPa of the set point by releasing gas to the flow meter as the hydrate dissociates.

Internal temperatures of hydrate samples were monitored by thermocouples over the duration of the experiments. Sample vessels either had one axially centered thermocouple or four thermocouples located along the top, middle, and bottom of the cylinder axis and midway along the sample side.[4,6] Chromel−alumel (Type K) thermocouples, referenced to either an ice/water calibration bath or a Hart Scientific Zero Point Calibrator (model 9101), measure sample temperatures to within ±0.1 K at 0.1 MPa. The experimental results in Figures 1−4 show the sample temperature measured by the middle thermocouple only. The temperature profiles near the sample surfaces are also discussed below.

Results

The relationship between the amount of hydrate dissociation and the internal sample temperature is illustrated in Figures 1 and 2. In temperature-scanning experiments, two changes occur as the sample temperature nears T_m: (1) the rate of dissociation of the remaining hydrate rises sharply, and (2) the rate of temperature increase in the sample decreases sharply while the external bath temperature continues to rise (Figures 1a, 1b, 2a, and 2b).[13] The sample temperature remains within a narrow temperature range, rising slowly with time as dissociation proceeds. This behavior defines the thermal buffering regime, and it is more pronounced and long-lived when the amount of remaining gas released from the hydrate sample exceeds a few percent (1a vs 1b). After some time interval, hydrate dissociation ceases, usually preceded by, but sometimes coincident with, a rise in sample temperature to T_m.

In fixed-temperature experiments, the samples are equilibrated at some temperature above T_m, then pressure is dropped rapidly to conditions outside the hydrate stability field, and dissociation begins immediately (Figures 1c, 2c). The sample temperature plummets below T_m due to both adiabatic cooling from gas expansion and the absorption of heat by hydrate dissociation. Adiabatic cooling results in a temperature decrease of about 4−6 K (for the typical P decrease in our experiments) and is short-lived (lasting ∼5 min). In experiments where T_{ext} is between 273 and 283 K, the temperature decrease initially undercools the thermal buffering regime, then rebounds to it within 2−15 min (rebound time decreases with increasing temperature). In experiments where $T_{ext} \geq 283$ K, the temperature drops directly to the buffering temperature regime (Figure 1c). Sample temperatures remain in the thermal buffering regime until dissociation nears completion, at which time the sample temperature rises to T_m. This behavior was observed in all

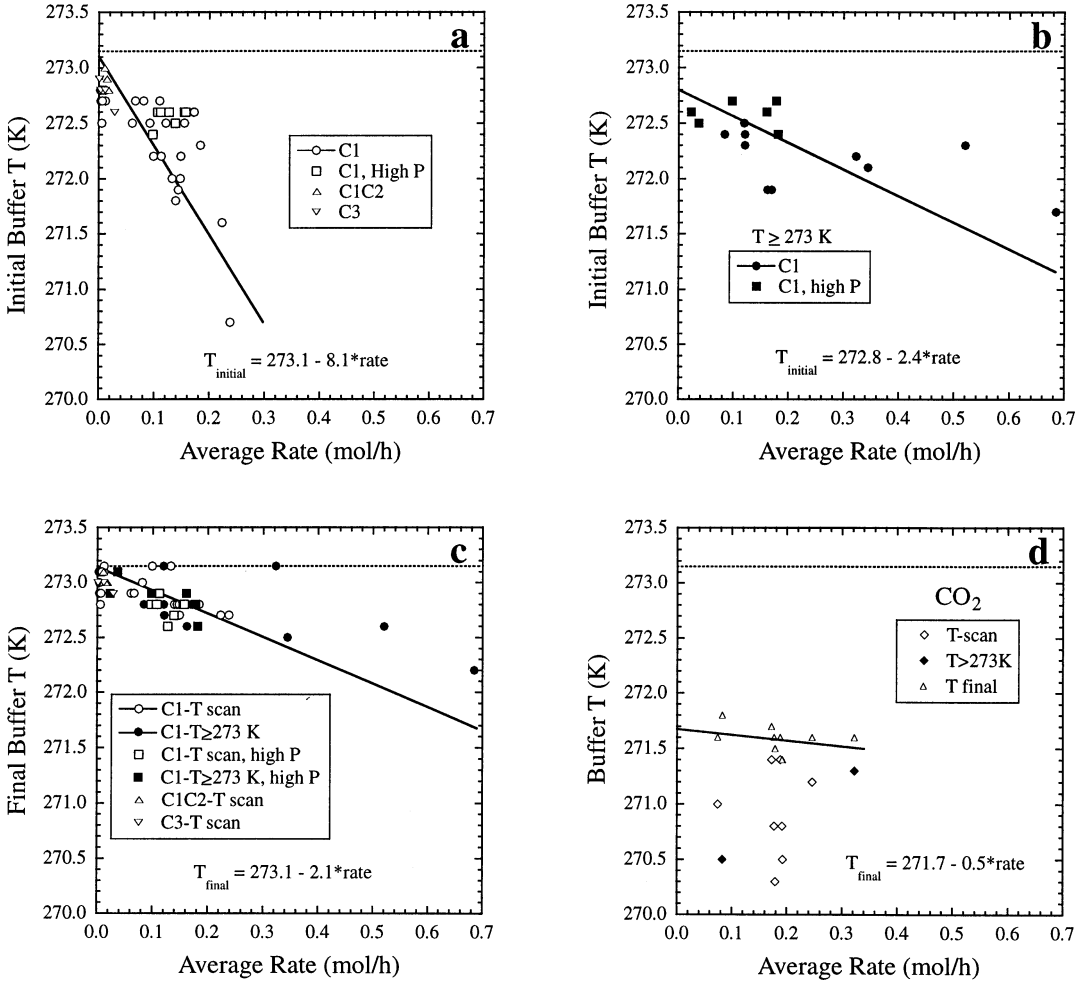

Figure 3. Relationship between initial or final buffering temperatures and the average dissociation rate. Dotted lines are positioned at T_m (H_2O at 0.1 MPa); in the elevated P experiments, T_m decreases to 273.08 and 273.01 K at 1.0 and 2.0 MPa, respectively. Panel a shows initial buffering temperatures in temperature-scanning experiments on C1, C1C2, and C3 hydrates at 0.1 MPa, and C1 at elevated pressures. Panel b shows initial buffering temperatures in fixed-temperature experiments on C1 hydrate at 0.1 MPa and elevated pressures. Panel c shows final buffering temperatures in all experiments on C1, C1C2, and C3 hydrates. Panel d shows initial and final buffering temperatures in temperature-scanning and fixed-temperature experiments on CO_2 hydrate at 0.1 MPa. Solid lines and equations are from least-squares fits to C1 hydrate data at 0.1 MPa (panels a and b), representing the broadest ranges of dissociation rates measured; these data sets were combined for the regression shown in panel c. Regressions serve merely to illustrate the general trends of decreasing buffering temperature with increasing dissociation rate (see text).

experiments conducted at bath temperatures above T_m (11 tests conducted between 273 and 289 K) and also in all tests conducted at elevated pressure conditions (6 tests conducted on C1 hydrate at 1.0 and 2.0 MPa). Additional details of the experiments at 0.1 MPa have been summarized previously.[4]

Similar behavior was observed in temperature-scanning and fixed-temperature experiments on CO_2 hydrate,[6] in which the sample rapidly dissociates to completion once T_{ext} exceeds T_m. CO_2 hydrate experiments show one notable difference: the buffering temperature range is depressed an additional 1−2 K below that observed for the hydrocarbon hydrates (Figures 1d, 2d).

Results on D_2O-host hydrates of C1, C1C2, C3, and CO_2 are fully consistent with the above observations on H_2O-host hydrates, although the buffering range was systematically shifted to higher temperatures in accordance with the higher melting point of D_2O. Average initial and final buffering temperatures and their offsets from T_m are categorized on the basis of experimental parameters and guest molecule composition in Table 1.

Rapid hydrate dissociation with thermal buffering just below T_m is observed in all of the experiments that we have performed to date at higher temperatures where T_{ext} exceeds T_m. Previously, Peters et al.[14] observed comparable thermal regimes and dissociation behavior in fixed-temperature experiments on C1 hydrate, and recently, Melnikov et al.[15] observed this behavior for C3 hydrate. In addition, similar dissociation behavior was observed calorimetrically for natural sII gas hydrate[16] as well as synthetic sII krypton gas hydrate,[17] where a sharp rise in dissociation rate is observed as samples are warmed through T_m.

To summarize, as the melting temperature of the material that comprises the hydrate framework is approached in temperature-scanning experiments, or when pressure is decreased to conditions outside the hydrate stability field in fixed-temperature experiments above 273 K, gas hydrates dissociate rapidly and completely in a narrow temperature range slightly below T_m. Our measurements also show that this buffering range depends directly on the composition of both the guest and hydrate host phases.

Discussion

The key to understanding the role of water in hydrate dissociation is the observed change in dissociation behavior as T_m is reached. In fixed-temperatures experiments above T_m,

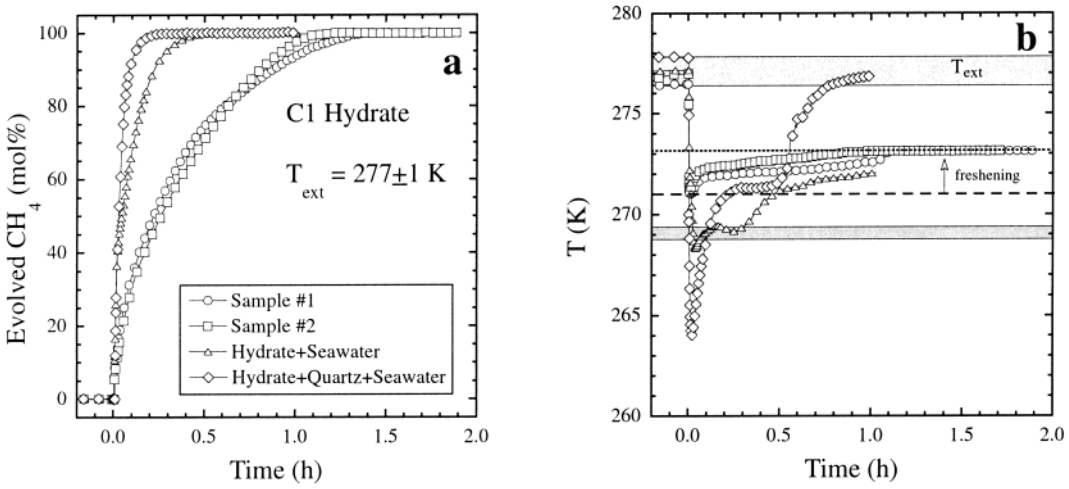

Figure 4. Gas release and thermal response of hydrate samples partially saturated with seawater (SMOW), following rapid depressurization to 0.1 MPa while maintaining at a fixed external temperature of 277 K. C1 hydrate in CH_4 gas atmosphere at 0.1 MPa (circle and square), C1 hydrate partially saturated with seawater (triangle), and C1 hydrate + 30% quartz by volume partially saturated in seawater (diamond) are compared (every fifth data point plotted). Panel a shows the evolution of gas over time. Dissociation ceased after 72 and 86 min in pure C1 hydrate (T_{ext} was 276.5 and 277.0 K, respectively), after 35 min in the hydrate + seawater sample, and in 18 min in the hydrate + quartz + seawater sample. Panel b shows the evolution of sample temperature over time, with the range of T_{ext} for all experiments indicated. The horizontal dotted line indicates T_m (273.15 K, pure H_2O), the horizontal dashed line indicates the calculated T_m for the seawater used (271 K, SMOW with a salinity of 35.2%), and the darker shaded region is the buffering regime near 269 K.

TABLE 1: Comparison of Average Buffering Temperatures to the Melting Points of H_2O and D_2O

experiment type[a]	n[b]	T_i (K) average[c]	$T_i - T_m$ H_2O[d]	$T_i - T_m$ D_2O[e]	T_f (K) average[c]	$T_f - T_m$ H_2O[d]	$T_f - T_m$ D_2O[e]
T-scan <6%	23	272.8 ± 0.1	−0.4	−0.2,−0.4	273.0 ± 0.1	−0.1	−0.1
T-scan >6%	24	272.3 ± 0.5	−0.9		272.8 ± 0.1	−0.3	
Fixed-T (≥ 273 K)	17	272.3 ± 0.3	−0.8		272.8 ± 0.2	−0.4	
CO_2	10	270.9 ± 0.4	−2.2	−1.8	271.6 ± 0.1	−1.6	−1.5

[a] Temperature-scanning experiments (see Figure 3a) were grouped on the basis of the amount of gas released from the hydrate while the sample temperature was buffered. The group that released <6% of the total gas content of the hydrate near T_m had average dissociation rates of less than 0.07 mol/h and includes results for C1, as well as all C1C2 and C3 hydrate experiments. The second T-scan group includes the remaining C1 experiments with higher average dissociation rates (including all high-pressure experiments below 273 K). Fixed T (Figure 3b) includes all C1 rapid depressurization experiments above 273 K at 0.1 MPa and higher pressures. T-scan and fixed-T experiments on CO_2 hydrate (Figure 3d) are grouped together. [b] Number of analyzed experiments on hydrates with H_2O-frameworks. [c] Average initial and final buffering temperatures (T_i and T_f, respectively) and their standard deviations for H_2O-framework hydrates. [d] Temperature difference between the average initial (or final) buffering temperature and the pure H_2O melting point (see text for discussion). [e] Temperature difference between the initial (or final) buffering temperature and the observed D_2O melting point. Note that, while pure D_2O is expected to melt at 277.0 K, observed melting temperatures were slightly depressed (to 275.7 K for CO_2, 276.1 K for C1, and 276.7 K for C1C2 and C3), possibly due to higher equilibrium solubilities of the gases in liquid D_2O.

hydrate dissociation is complete in minutes to hours, occurring in narrow temperature ranges below T_m that are independent of T_{ext}.[4] Dissociation rates increase with increasing T_{ext} and higher heat flow from the external bath. But at temperatures below T_m, the dissociation rate is highly varied among hydrates and is highly temperature-dependent for methane hydrate (Table 2). However, when subsequently warmed through T_m, all remaining gas is released from the partially dissociated hydrate samples. This behavior is independent of the previous $P-T$ history, dissociation rate, and state of sample dissociation, as well as the hydrate structure and composition. Dissociation goes to completion quickly while sample temperatures are buffered in the same interval below T_m that is observed in the fixed-temperature experiments.

As discussed in ref 6, when warming partially dissociated hydrate samples from temperatures below T_m, preexisting barriers to hydrate dissociation disappear as the temperature reaches the H_2O solidus, suggesting that the formation of liquid water is key to rapid and complete breakdown of the hydrate. These results point to gas diffusion as the rate-limiting process at lower temperatures and indicate that ice product plays some role in retarding hydrate dissociation. Heat flow into the sample is ruled out as the rate-limiting process below T_m; for both C1 (242−272 K) and CO_2 hydrates, samples are in thermal equilibrium with the external bath when depressed dissociation rates are observed, and rates do not increase systematically with increasing T_{ext}. Instead, hydrate dissociation behavior seems to depend foremost on the guest molecule(s) present (Table 2). The range in dissociation rates for hydrates of different composition and structure highlights the fact that the mere presence of ice as a gas shielding or sealing mechanism is insufficient to account for all of the experimental results.[12] A unifying theory that integrates the roles of ice, temperature, and guest molecule and explains the complexity of dissociation behavior observed for various hydrates following different $P-T$ pathways below T_m remains elusive.

The rapid release of all remaining gas from the hydrate samples once the external bath temperature exceeds T_m indicates that dissociation is producing liquid water under these conditions, even though the sample temperature is buffered below T_m. We attribute the observed thermal buffering during dissociation to the crossing of the solid/liquid boundary of H_2O or D_2O and not to the hydrate dissociation reaction itself, since the P, T conditions do not coincide with known or extrapolated

TABLE 2: Extent of Gas Hydrate Dissociation along Various $P-T$ Pathways below or above T_m[a]

hydrate composition	heating from below T_{eq} ($T < T_m$)[b]	rapid depressurization[c] $T_{ext} < T_m$	rapid depressurization[c,d] $T_{ext} > T_m$
C1 (sI)	>95%	>90% (T_{ext} < 240 K) <50% (242−272 K)[e]	100%
CO_2 (sI)	<10%	<20%[f]	100%
C1C2 (sII)	>95%	>95%[g]	100%[h]
C3 (sII)	>95%		100%

[a] Extent of dissociation (in %) after up to 4 h at defined conditions. [b] Heating under isobaric conditions of 0.1 MPa. Gas yields obtained within 25 K (C1,[5] C1C2,[12] CO_2[6] K) or 10 K (C3) of T_{eq}, the temperature of the hydrate phase boundary. Gas yields for CO_2 hydrate are less than 20% for T up to 270 K.[6] [c] Rapid depressurization to 0.1 MPa. [d] C1,[4,14] C3,[15] and CO_2[6] hydrate release 100% of their gas contents while internal sample temperatures remain buffered ~1 (C1, C3) to 2 K (CO_2) below T_m. [e] Dissociation rates are depressed up to 4 orders of magnitude below those at lower temperatures, such that 50% of the sample remains after a few hours (242 K) to a few weeks (268 K).[5,12] At elevated pressures, dissociation rates are depressed further in this temperature range. [f] Maximum amount released following depressurization and isothermal hold for 0.3 to 3.8 h (T_{ext} 240−268 K), followed by heating to 270 K. [g] At 268 K, the gas is released in minutes. [h] Assumed on the basis of release of all remaining gas from partially dissociated samples once T_{ext} exceeds T_m.

hydrate reaction boundaries. Note that, at the ice point, the endothermic enthalpy of dissociation for the reaction

$$M{\cdot}nH_2O(s) = M(g) + nH_2O(l) \quad (1)$$

where "M" is the guest molecule, is more endothermic by $n \times 6.01$ kJ/mol·H_2O (the enthalpy of melting of H_2O) than when $H_2O(s)$ is the product.[17,18] The enthalpy of reaction is independent of whether hydrate dissociates to gas + ice that then melts, or to gas + water directly. Subsequent freezing of water product and an ample supply of heat from the warmer, external bath can offset the larger enthalpy required to produce water during dissociation.

Localized freezing of the water product of dissociation is also consistent with the distribution of ice following the end of dissociation.[4] We know that ice forms at some stage in the process in every experiment, both from direct observation of abundant ice product following dissociation and from the observed buffering temperature at T_m once hydrate dissociation ceases.[4,14] While dissociation proceeds throughout the sample, progressing on a localized scale inward from hydrate grain surfaces exposed in free pore space (as indicated by the immediate, sample-wide onset of the thermal buffering behavior), we also know, from the observed temperature profiles,[4,13] that the extent of hydrate dissociation is heterogeneous between the sample surfaces and interior. Concurrent with continued dissociation in the sample interior, dissociation goes to completion at the sample surfaces, and the heat flow from the external bath induces preferred ice melting at T_m along sample surfaces. We have shown previously[4] that the rate of C1 hydrate dissociation in fixed-temperature experiments above T_m is proportional to the heat flow from the warmer external bath to the sample interior. This conclusion is based on an estimated heat flow budget that assumed heat flow primarily through the direct contact of the sample base with the enclosing metal sample chamber (this is specific to our apparatus configuration). Peters et al.[14] observed comparable results but with a different final distribution of ice due to the canted position of their pressure vessel. They successfully reproduced both the observed temperature profile and dissociation behavior with a model that assumes radial conduction of heat through two moving boundaries of hydrate + ice (inner boundary) and ice + water (outer boundary). In high temperature (>280 K) experiments, high heat flow produces such rapid dissociation that the onset of buffering occurs only in the sample interior and well into the dissociation event, and buffering is short-lived.[4]

We hypothesize that the buffering behavior arises from the freezing of water produced by hydrate dissociation, but the specific characteristics of the observed buffering temperature ranges require further discussion. (1) Buffering temperatures are systematically offset below T_m. (2) The buffering temperature is not constant, but rises (up to 1.3 K) over time. (3) The temperature range depends on the hydrate composition (H_2O vs D_2O, hydrocarbons vs CO_2). And (4), the initial buffering temperature correlates with the average rate of dissociation near T_m (Figure 3). Specifically, the initial buffering temperature data for C1 hydrate at 0.1 MPa appear to fall along two distinct trends depending on whether the experiment involved temperature-scanning (Figure 3a) or fixed-temperature (Figure 3b) conditions. In both cases, however, the initial buffering temperature decreases as the average rate of dissociation increases. The shallower slope of the fixed-temperature data is strongly influenced by the four 0.1 MPa experiments at $T_{ext} \geq 279$ K which had average dissociation rates >0.3 mol/h. The correlation between decreasing buffering temperatures with increasing dissociation rate is also reflected in the final buffering temperatures (Figure 3c), which again show a negative correlation with respect to dissociation rate, but fall within a narrower range (Table 1). For the remaining experiments on hydrocarbon hydrates, both the initial and final buffering temperatures fall along the trends previously described, while the observed dissociation rates fall within a much narrower range. Last, the data for CO_2 hydrate do not exhibit an obvious correlation between initial buffering temperature and dissociation rate (Figure 3d), and the offset from T_m is greater for comparable dissociation rates. It is important to remember that the measured sample temperature reflects the average value imposed by the surrounding material, and that, along with local sample variability,[13] may give rise to the scatter in the data. Nonetheless, the trend of decreasing buffer temperature with increasing average dissociation rate is indicated.

We hypothesize that the buffering temperature is depressed below T_m due to freezing point depression arising from the presence of dissolved guest gas molecules in liquid water. This colligative property is independent of the specific dissolved species, depending only on the amount of solute. The relationship between the mole fraction of the dissolved species in the liquid and the freezing point depression is described by

$$x_{solute} = -(\Delta H_m/R) * (1/T_{buffer} - 1/T_m) \quad (2)$$

where ΔH_m is the enthalpy of fusion, T_{buffer} is the depressed melting point, and T_m is the melting point of the pure solvent. This equation assumes that solid solution does not occur in the solid phase of the solvent, which is a reasonable assumption for H_2O and D_2O ices. Table 3 summarizes the observed ranges of buffering temperatures in different experiments and the calculated concentrations of dissolved gas required to produce the observed freezing point depression. The equilibrium gas concentrations at 0.1 MPa, 273.15 K have been calculated from Henry's Law constants.[19] We have also calculated the "concentration" of gas in the gas hydrate after converting the hydrate framework to liquid water at 273.15 K. This provides an upper bound on the maximum gas concentration possible if the hydrate

TABLE 3: Comparison of Calculated Concentrations of Hydrate Guest Species in Liquid Water on the Basis of the Observed Freezing Point Depression of H_2O, Equilibrium Conditions, and the Concentration in Gas Hydrate

experiment description[a]		buffer T range[b] (K)	solubility from ΔT_m[c] (mol/L H_2O)	equilibrium solubility[d] (mol/L H_2O)	hydrate gas concentratio[e] (mol/L H_2O)
T-scan <6%	T_i	273.0 to 272.5	0.081 to 0.353	0.0025	9.423
	T_f	273.15 to 272.8	0.000 to 0.189		
T-scan >6%	T_i	272.7 to 270.7	0.243 to 1.362	0.0025	9.423
	T_f	273.15 to 272.6	0.000 to 0.298		
$T \geq 273$ K	T_i	272.7 to 271.7	0.243 to 0.795	0.0025	9.423
	T_f	273.15 to 272.2	0.000 to 0.517		
CO_2	T_i	271.4 to 270.3	0.963 to 1.593	0.0756	9.652
	T_f	271.8 to 271.4	0.739 to 0.963		

[a] See Table 1 for detailed descriptions. [b] Ranges of observed initial and final buffering temperatures, as opposed to the averaged values shown in Table 1. [c] Calculated amount of dissolved gas based on the observed freezing point depression of H_2O (see text). [d] Equilibrium concentration of hydrate-forming gases in liquid water at 0.1 MPa and 273.15 K. Values are calculated from the Henry's Law constants summarized by Sloan[19] and the relationship $X_{gas} = P/H_{gas}$. Equilibrium concentrations of ethane and propane at 273.15 K are 0.0044 and 0.0040 mol/L H_2O, respectively. [e] Hypothetical gas concentration in proportions found in gas hydrate, i.e., concentration if hydrate breaks down to gas + liquid H_2O and no movement of gas occurs. Assumes hydrate stoichiometry "*n*" numbers of 5.89 (C1[5,8]), 5.78 (C1C2[9]), 17 (C3, assumed), and 5.75 (CO_2[6]). Concentrations for C1 and CO_2 hydrates are shown; concentrations of C1C2 hydrate and C3 hydrate are 9.602 and 3.265 mol/L H_2O, respectively.

instantly converts to gas + water with no exsolution of the guest molecules from the water to form a discrete gas phase.

The gas concentrations required to produce the observed freezing point depressions are one to two orders of magnitude greater than the equilibrium concentrations but much less than the concentration of gas in the hydrate. Such gas concentrations could arise as follows: immediately upon dissociation, a solution of gas and water at higher-than-equilibrium concentration forms before freezing excludes the dissolved gas. This model of depression of the melting temperature of ice by gas solution is also consistent with the observation that the buffering temperature increases over time, i.e., the freezing point depression decreases as the hydrate dissociation rate decreases. This is supported by the asymmetry of the flow rate curves with respect to the buffering temperature interval (Figure 2). Once dissociation slows and then ceases, this posited supersaturated solution should rapidly tend toward equilibrium, confirmed by the observed shift in sample temperature to T_m.

The temperature offsets from T_m observed for the CO_2 system are always greater than those observed for the hydrocarbon gases (Figures 1 and 3, Table 1) in both H_2O- and D_2O-host systems. Since CO_2 is 30 times more soluble in water than methane gas at equilibrium conditions (Table 3), this is not surprising. However, the relative solubility difference inferred from the buffering temperatures during dissociation is much less. When experimental conditions and dissociation rates are comparable (0.06−0.22 mol/h in Figure 3a and 3d; C1, T-scan >6% lost vs CO_2 in Table 3), the gas concentrations calculated from the freezing point depressions are only 2−5 times higher for CO_2. This result is entirely consistent with our hypothesis. Since C1 and CO_2 hydrate have similar gas "concentrations", at comparable dissociation rates the amount of dissolved gas, and therefore the observed freezing point depression, should be similar. Thus hydrate dissociation produces the high, non-equilibrium gas concentrations, and secondarily, the higher activity of methane in water probably promotes its more rapid exsolution, maintaining the observed difference in solubility.

Alternatively, if one does not accept that hydrate is dissociating to gas + water for the reasons outlined at the start of the discussion (namely, the relationship between temperature, dissociation rates, and the H_2O solidus), one must still explain the observed freezing point depression with respect to hydrate dissociation to gas + ice. In this case, the product phases would already be separated, as impurities are not easily incorporated into the crystalline ice structure. To lower the H_2O melting temperature, either the chemical potential of the water phase must still be lowered by gas solution, or the chemical potential of the ice produced upon dissociation must be higher. In the former case, an additional mechanism, such as localized, highly elevated gas pressures (tens of MPa), would be required to elevate gas concentrations well above equilibrium values to produce the freezing point depression as ice product melted. This added complexity is not supported by the experimental data nor by the fact that ice is weakest at these temperatures.[20] In the latter case, we have no evidence to support the formation of an "ice-like" phase with a higher chemical potential than pure ice Ih. The measured difference in the enthalpy of dissociation is equal to $n \times 6.01$ kJ/mol·H_2O within experimental error.[17] If the "ice-like" phase had a higher entropy than that of pure ice Ih, this would actually *raise* the melting point. Furthermore, this scenario is inconsistent with the fact that internal sample temperatures quickly shift to T_m of pure H_2O once dissociation ceases, where ice melting at T_m can continue for hours.

An important question that remains is whether this behavior is relevant to a marine setting, where hydrate is in contact with excess seawater, not hydrate-forming gas. We have obtained limited experimental dissociation data on C1 hydrate that has been partially saturated by pressurized, methane-saturated seawater introduced into the sample chamber from the top after hydrate synthesis. Some secondary growth of C1 hydrate occurred, and the seawater did not completely saturate the sample to the bottom. In fixed-temperature experiments at 277 K, the dissociation rate is higher in seawater-saturated samples, and the buffering temperatures are depressed to even lower temperatures (Figure 4). The buffering temperature is near 269 K during dissociation of the seawater-only sample, and then rises to 271 to 272 K once dissociation is complete (Figure 4b). A 1−2 K depression of the ice melting temperature would correspond to 0.6 to 1.2 mol/L H_2O of dissolved material, wholly consistent with the salinity of the seawater as it "freshened" with the melting of ice product. The further depression of the freezing point by 2 K (buffering during dissociation at 268.9−269.5 K, average rate 0.52 mol/h) would correspond to the additional solution of 1.2 to 0.8 mol of CH_4/L of H_2O. This temperature offset from the baseline seawater melting temperature is greater than that observed at comparable rates in the seawater-free experiments (Figure 3b). In the hydrate + quartz + seawater experiment, thermal buffering during dissociation is not indicated by the data; however, half of the sample dissociated in a minute, driving the temperatures as low as 264 K, and the temperature rebounded steadily as the remaining

gas was released. Nonetheless, the experimental evidence that we discuss above suggests that thermal buffering and freezing point depression arising from gas solution are also relevant to hydrate dissociation in seawater-bearing systems under certain conditions.

Conclusion

When gas hydrate, at 0.1 MPa, is warmed to temperatures above the melting point of ice, all remaining gas is released in a single event within a well-defined temperature range just below T_m until no hydrate remains. Similarly, when gas hydrate is destabilized at external temperatures above T_m by decreasing the pressure below the hydrate stability boundary, the hydrate dissociates completely while sample temperatures are buffered in the same ranges below T_m. The fact that no hydrate persists once temperatures exceed the melting point of the hydrate network-forming material indicates that existing barriers to hydrate dissociation disappear when dissociation produces water instead of ice. These observations apply to both sI and sII gas hydrates containing alkanes (C1−C3) and CO_2, by far the most common hydrate compositions in nature, as well as to sII Kr hydrate.[17] It remains to be seen if such behavior is generally applicable to gas hydrates.

We have hypothesized that the well-defined temperature ranges observed during dissociation are due to thermal buffering as the water product freezes, and temperatures are depressed below T_m due to the presence of dissolved dissociated gas in the water product. The corresponding freezing point depression increases with the rate of dissociation and with the relative solubilities of the hydrate-forming gases, with calculated concentrations falling between equilibrium values and the upper bound of the gas concentration in the hydrate. Our hypothesis is based on both macroscopic observations and thermodynamic principles. Specifically, we consider the thermal history of the sample during dissociation, the distribution of phases, the heat flow in the system, the relationship to known equilibrium boundaries, and the factors that can shift their P, T position (i.e. freezing point depression). The hypothesis needs to be tested further using techniques that can resolve these processes at a microscopic scale, possibly using an optical cell, Raman spectroscopy, or nuclear magnetic resonance (NMR) spectroscopy.

The dissociation behavior near T_m has been observed in samples that range in mass from 1 to 100 g, where our samples fall in the middle of this range. While the thermal buffering behavior also is observed in samples larger than ours,[14,15] we expect that it may not occur when the ratio of the sample surface to volume is sufficiently high, for example in very small samples, samples with relatively low hydrate content (compared to sediment, water, and/or free gas), or when the ratio of length to cross-sectional area is very low or high. In these cases, dissociation and heat transfer could be sufficiently rapid, such that the dynamic balance between hydrate dissociation and water product solidification necessary for thermal buffering is not reached before dissociation goes to completion. As we have noted, in our experiments the duration of thermal buffering is dependent on location within the sample[13] and on the amount of temperature overstep of T_m.

Last, it is important to note that thermal buffering near the H_2O or D_2O melting point is observed during gas hydrate dissociation at pressures below the quadruple point (Figure 5). Above the quadruple point, the gas hydrate phase boundary lies at higher temperatures than the H_2O solidus, and dissociation proceeds at temperatures fixed at the hydrate stability boundary.

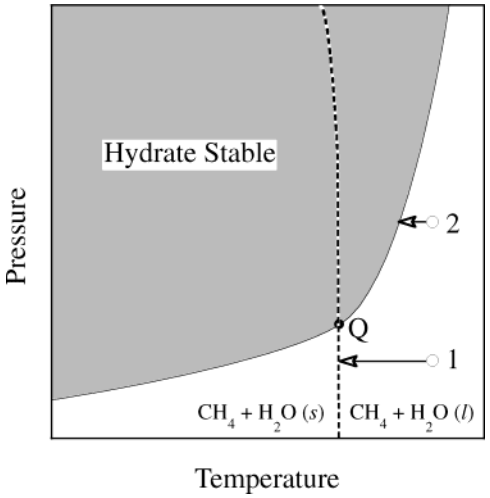

Figure 5. Schematic P, T phase diagram for gas hydrate, showing hydrate stability field (shaded area); the quadrupole point Q, where hydrate + gas + water + ice are in equilibrium; the melting curve for H_2O (dotted line); and the starting conditions of two dissociation experiments (open circles). Under fixed pressure conditions, dissociation rapidly cools the sample until sample temperatures intersect either the H_2O melting curve (#1; i.e., this study) or the hydrate equilibrium boundary (#2), where they are buffered as dissociation proceeds. Note that, in case #1, the buffering temperatures are actually just below the melting curve (see text for complete discussion).

Acknowledgment. This manuscript benefited greatly from discussions with E. Dendy Sloan and Simon L. Marshall. William B. Durham, E. Dendy Sloan, and two anonymous referees provided helpful reviews of the manuscript. This work was performed under the auspices of the contract: "Fundamental physical properties and stability of carbon dioxide clathrate", awarded to Lawrence Livermore National Laboratory from the DOE/NETL Carbon Sequestration Program.

References and Notes

(1) Westbrook, G. K.; Carson, B.; Musgrave, R. J.; et al. *Proc. of the ODP, Init. Rep.* **1994**, *146*.

(2) Kastner, M.; Kvenvolden, K. A.; Whiticar, M. J.; Camerlenghi, A.; Lorenson, T. D. *Proc. of ODP, Sci. Res.* **1995**, *146*, 175.

(3) Paull, C. K.; Matsumoto, R.; Wallace, P. J.; et al. *Proc. of the ODP, Init. Rep.* **1996**, *164*.

(4) Circone, S.; Stern, L. A.; Kirby, S. H.; Pinkston, J. C.; Durham, W. B. In *Gas Hydrates: Challenges for the Future*; Holder, G., Bishnoi, P., Eds.; New York Academy of Sciences: New York, 2000; p 544.

(5) Stern, L. A.; Circone, S.; Kirby, S. H.; Durham, W. B. *J. Phys. Chem. B* **2001**, *105*, 1756.

(6) Circone, S.; Stern, L. A.; Kirby, S. H.; Durham, W. B.; Chakoumakos, B. C.; Rawn, C. J.; Rondinone, A. J.; Ishii, Y. *J. Phys. Chem. B* **2003**, *107*, 5529.

(7) Stern, L. A.; Kirby, S. H.; Durham, W. B. *Science* **1996**, *273*, 1843.

(8) Circone, S.; Kirby, S. H.; Pinkston, J. C.; Stern, L. A. *Rev. Sci. Instrum.* **2001**, *72*, 2709.

(9) Helgerud, M. B.; Circone, S.; Stern, L. A.; Kirby, S. H.; Lorenson, T. D. Proceedings of the 4th International Conference on Gas Hydrates, Yokohama, Japan, 2002, p 716.

(10) Rawn, C. J.; Rondinone, A. J.; Chakoumakos, B. C.; Marshall, S. L.; Stern, L. A.; Circone, S.; Kirby, S. H.; Jones, C. Y.; Toby, B. H.; Ishii, Y. Proceedings of the 4th International Conference On Gas Hydrates, Yokohama, Japan, 2002, p 595.

(11) Rawn, C. J.; Rondinone, A. J.; Chakoumakos, B. C.; Circone, S.; Stern, L. A.; Kirby, S. H.; Ishii, Y. *Can. J. Phys.* **2003**, *81*, 431.

(12) Stern, L. A.; Circone, S.; Kirby, S. H.; Durham, W. B. *J. Can. Phys.* **2003**, *81*, 271.

(13) The temperatures near the sample surfaces (top, bottom, and side) are not shown in Figures 1 and 2 for simplicity, but are briefly summarized here. In both temperature-scanning and fixed-temperature experiments, the temperature near the sample top closely tracks that near the sample middle,

although its subsequent rise to T_m often precedes that observed at the sample middle. In temperature-scanning experiments, the sample bottom temperature may stall in the buffering range, but this is short-lived relative to the thermal buffering of the sample interior. This is also true in fixed-temperature experiments below 274 K. At warmer conditions, however, the bottom temperatures plunge below 273 K, then rise steadily back to, or through, T_m.[4] The temperature at the sample side often closely tracks that at the sample bottom, but in some experiments it has tracked the middle temperature when the thermocouple position was shifted in towards the sample interior. The relationships described above are representative of the majority of the experiments, although some exceptions and variations do exist. This is not surprising, given that temperature is measured at point locations in the sample. Minor sample-to-sample variability in thermocouple positioning, heat transfer, and sample porosity can have measurable effects on the observed temperature profiles.

(14) Peters, D.; Selim, M. S.; Sloan, E. D. In *Gas Hydrates: Challenges for the Future*; Holder, G., Bishnoi, P., Eds.; New York Academy of Sciences: New York, 2000; p 304.

(15) Melnikov, V. P.; Nesterov, A. N.; Reshetnikov, A. M. Proceedings of the 8th International Conference on permafrost, Zurich, Switzerland, July 21−25, 2003.

(16) Davidson, D. W.; Garg, S. K.; Gough, S. R.; Handa, Y. P.; Ratcliffe, C. I.; Ripmeester, J. A.; Tse, J. S. *Geochim. Cosmochim. Acta* **1986**, *50*, 619.

(17) Handa, Y. P. J. *Chem. Thermodynamics* **1986**, *18*, 891.

(18) Handa, Y. P. J. *Chem. Thermodynamics* **1986**, *18*, 915.

(19) Sloan, E. D. *Clathrate Hydrates of Natural Gases*, 2nd ed; Marcel Dekker: New York, 1998.

(20) Durham, W. B.; Stern, L. A. *Annu. Rev. Earth and Planetary Sci.* **2001**, *29*, 295.